

SCIENTIFIC REPORTS



OPEN

Growth and structural characterisation of Sr-doped Bi₂Se₃ thin films

Meng Wang^{1,4,6}, Dejong Zhang², Wenxiang Jiang³, Zhuojun Li^{1,4,6}, Chaoqun Han³, Jinfeng Jia^{3,5}, Jixue Li², Shan Qiao^{1,4,6}, Dong Qian^{3,5}, He Tian² & Bo Gao^{1,4,6}

We grew Sr-doped Bi₂Se₃ thin films using molecular beam epitaxy, and their high quality was verified using transmission electron microscopy. The thin films exhibited weak antilocalisation behaviours in magneto-resistance measurements, a typical transport signature of topological insulators, but were not superconducting. In addition, the carrier densities of the non-superconducting thin-film samples were similar to those of their superconducting bulk counterparts. Atom-by-atom energy-dispersive X-ray mapping also revealed similar Sr doping structures in the bulk and thin-film samples. Because no qualitative distinction between non-superconducting thin-film and superconducting bulk samples had been found, we turned to a quantitative statistical analysis, which uncovered a key structural difference between the bulk and thin-film samples. The separation between Bi layers in the same quintuple layer was compressed whereas that between the closest Bi layers in two neighbouring quintuple layers was expanded in the thin-film samples compared with the separations in pristine bulk Bi₂Se₃. In marked contrast, the corresponding changes in the bulk doped samples showed opposite trends. These differences may provide insight into the absence of superconductivity in doped topological insulator thin films.

Topological insulators (TIs) and superconductors (TSCs) are active research fields in condensed matter physics¹. The ability of TSCs to host gapless Majorana-type collective excitations^{2,3}, which can serve as building blocks for fault-tolerant topological quantum computing^{4–6}, has sparked substantial research interest. One possible route to obtain TSCs is to dope TIs. To date, superconductivity has been successfully induced in doped TIs such as Cu-, Sr-, and Nb-doped Bi₂Se₃^{7–9}. A few signs of topological superconductivity have been observed in these materials. For example, point contact spectroscopy measurements have revealed a zero-bias conductance peak (ZBCP) in Cu-doped Bi₂Se₃, suggesting a possible mid-gap state that may be related to the Majorana zero mode¹⁰. Signs of odd-parity superconductivity have also been inferred from various measurements including nuclear magnetic resonance experiments and angle-dependent specific heat measurements^{11,12}. However, contradictory results have also been reported. A scanning tunnelling spectroscopy study of Cu-doped Bi₂Se₃ did not reproduce the finding of ZBCP¹³. The key problem is the relatively low superconducting volume fraction (~40%)^{7,14–17} and large superconducting inhomogeneity in single crystals^{13,16}. To search for smoking-gun type evidence of Majorana zero modes, a number of detection schemas have been proposed, many of which require the preparation of superconducting films from doped TIs^{18–22}. Unfortunately, attempts to grow superconducting doped TI films have not yet been successful^{23–25}. The superconductivity in Cu-doped Bi₂Se₃ was initially believed to originate from the intercalation of Cu dopant atoms into van der Waals (vdW) gaps. However, although Cu intercalation was successfully realised in Bi₂Se₃ thin films grown by molecular beam epitaxy (MBE), the Cu-doped Bi₂Se₃ films were not superconducting²³. Here, we report our attempt to grow Sr-doped Bi₂Se₃ thin films using MBE. High-resolution

¹CAS Center for Excellence in Superconducting Electronics (CENSE), Shanghai, 200050, China. ²Center of Electron Microscopy and State Key Laboratory of Silicon Materials, School of Materials Science and Engineering, Zhejiang University, Hangzhou, 310027, China. ³Key Laboratory of Artificial Structures and Quantum Control (Ministry of Education), School of Physics and Astronomy, Shanghai Jiao Tong University, Shanghai, 200240, China. ⁴State Key Laboratory of Functional Materials for Informatics, Shanghai Institute of Microsystem and Information Technology, Chinese Academy of Sciences, 865 Changning Road, Shanghai, 200050, China. ⁵Collaborative Innovation Center of Advanced Microstructures, Nanjing, 210093, China. ⁶University of Chinese Academy of Sciences, Beijing, 100049, China. Meng Wang, Dejong Zhang and Wenxiang Jiang contributed equally to this work. Correspondence and requests for materials should be addressed to D.Q. (email: dqian@sjtu.edu.cn) or H.T. (email: hetian@zju.edu.cn) or B.G. (email: bo_f_gao@mail.sim.ac.cn)

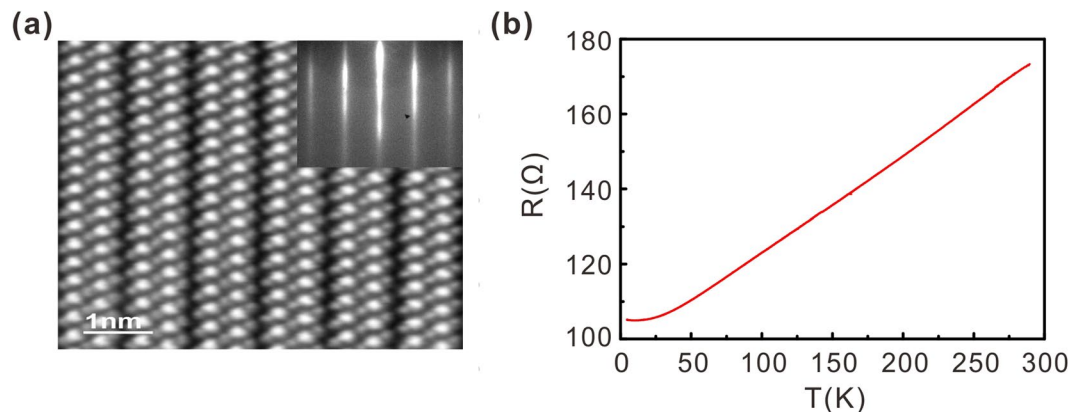


Figure 1. Structural and electrical characterisation of Sr-doped Bi_2Se_3 thin films. (a) Cross-sectional HRTEM image of a film clearly showing the quintuple-layer structure. Inset: Resolved RHEED pattern of a Sr-doped Bi_2Se_3 thin film. (b) Typical temperature dependence of the resistance of Sr-doped Bi_2Se_3 thin films.

high-angle annular dark-field scanning transmission electron microscopy (HAADF-STEM) examination verified the high quality of the films. In addition, magneto-resistance measurements revealed a weak antilocalisation (WAL) behaviour, which is a typical transport signature of TIs^{26–30}, indicating the well-preserved topological surface state. Similar to Cu-doped Bi_2Se_3 thin films, the Sr-doped Bi_2Se_3 thin films were not superconducting, although the carrier densities of the films were similar to those of superconducting bulk $\text{Sr}_x\text{Bi}_2\text{Se}_3$ samples^{8,31}. To explore the differences between the non-superconducting thin films and superconducting bulk samples, we performed atom-by-atom energy-dispersive X-ray spectroscopy (EDX) mapping. Similar Sr doping structures were observed in both types of samples. The only difference was the opposite trend of expansion/compression of the separation between Bi layers in the Bi_2Se_3 lattice for the bulk and thin-film doped samples (compared with that in pristine Bi_2Se_3), which suggests that the emergence of superconductivity in doped Bi_2Se_3 is possibly related with doping-induced lattice structural change.

Results

Structural and electrical characterisation of Sr-doped Bi_2Se_3 thin films. Sr-doped Bi_2Se_3 thin films were grown using MBE, and HAADF-STEM was used to inspect the film quality. Figure 1a presents a HAADF-STEM image of a thin-film sample, clearly revealing the typical quintuple-layer structure of Bi_2Se_3 . The bright columns correspond to Bi atoms with high atomic number. The Sr dopant atoms are difficult to detect in the HAADF-STEM image because of the low Sr concentration of the sample and the low atomic number of Sr. The inset of Fig. 1a presents a reflection high-energy electron diffraction (RHEED) pattern of an approximately 50-nm-thick film, which confirms the high film quality. To determine whether the thin-film sample was superconducting similar to bulk Sr-doped Bi_2Se_3 , we performed resistance versus temperature (R–T) measurements, as shown in Fig. 1b. The R–T measurements do not reveal any sign of superconducting behaviour.

The carrier densities in the Sr-doped thin-film samples were determined using Hall measurements. Figure 2a presents the Hall resistivity curves of two thin-film samples. The carrier densities deduced from the linear fitting of the curves were $1.11 \times 10^{20} \text{ cm}^{-3}$ and $5.67 \times 10^{19} \text{ cm}^{-3}$ at 5 K, respectively. These numbers are close to the typical carrier density of bulk superconducting Sr-doped Bi_2Se_3 samples^{8,31}. In addition, a prominent cusp of magneto-conductivity was observed near zero magnetic field at 5 K, as shown in Fig. 2b. The cusp can be attributed to WAL behaviour, which is a typical transport signature of two-dimensional topological surface states and has been observed in many transport measurements of TI thin films^{26–30}. Usually the WAL behaviour can be analysed using the Hikami–Larkin–Nagaoka (HLN) quantum interference model³². We also noticed that Adroguer *et al.* has proposed a new model to describe the quantum correction to conductivity, which accounts for the Dirac nature of the surface state while HLN model considers a quasi-two-dimensional electron gas with parabolic electron dispersion^{33,34}. Because the carrier density of thin-film samples is in the order of $10^{19} \sim 10^{20} \text{ cm}^{-3}$, the Fermi level (approximately 320–400 meV above the Dirac Point) crosses with the bulk conduction band according to our previous angle-resolved photoemission spectroscopy (ARPES) measurement results on bulk Sr-doped Bi_2Se_3 samples with similar carrier density³⁵. In this condition, the HLN model can still be applied to our samples:

$$\Delta\sigma_{xx}(B) = -\alpha \cdot \frac{e^2}{\pi h} \left[\psi \left(\frac{1}{2} + \frac{B_\phi}{B} \right) - \ln \left(\frac{B_\phi}{B} \right) \right] \quad (1)$$

where $\Delta\sigma_{xx}(B) = \sigma_{xx}(B) - \sigma_{xx}(0)$ represents the variation of two-dimensional magneto-conductivity, α is the WAL coefficient, ψ is the digamma function, and $B_\phi = \frac{\hbar}{4el_\phi^2}$ is the effective magnetic field characterised by the dephasing length l_ϕ . The α value can be 0.5 or 1 depending on the number of topologically protected transport channels. In addition to the cusp near zero magnetic field, the magneto-resistance measurements also revealed a linear magnetic field dependence, as fitted in the inset of Fig. 2b. This linear magneto-resistance behaviour has been observed in many transport measurements of TIs and has been attributed to the scattering of Dirac electrons

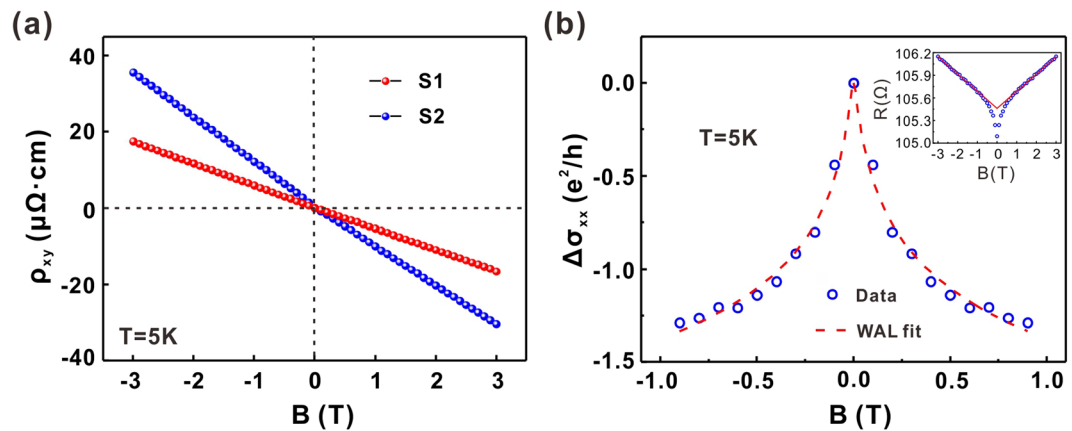


Figure 2. Hall measurements and WAL behaviour of Sr-doped Bi_2Se_3 thin films. **(a)** Hall resistivity versus magnetic field of two Sr-doped Bi_2Se_3 thin films measured at 5 K. **(b)** WAL behaviour of the thin films at 5 K. The red dashed line in the low-magnetic-field region is a WAL fit to the magneto-conductivity, which was subtracted by the conductivity background deduced from the extrapolating linear magneto-resistance towards zero magnetic field. Inset: The red solid line is a linear fit to the magneto-resistance in the region of magnetic field $|B| \geq 1\text{ T}$, which contributes the conductivity background from the bulk.

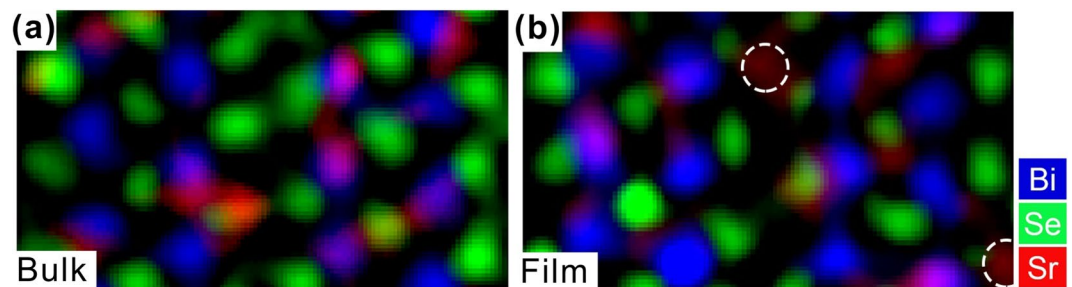


Figure 3. EDX mappings of bulk and thin-film samples. **(a)** EDX mapping for superconducting $\text{Sr}_{0.05}\text{Bi}_2\text{Se}_3$ bulk sample and **(b)** Non-superconducting thin-film $\text{Sr}_{0.13}\text{Bi}_2\text{Se}_3$ sample. The white dashed circles denote the Sr dopant atoms located in vdW gaps.

in the surface transport channel and the impurity scattering of the electrons in the bulk transport channel^{27,28,36–38}. To achieve a better fit for the WAL behaviour, we subtracted the conductivity deduced from the linear magneto-resistance background from the raw data by extrapolating the linear magneto-resistance towards zero magnetic field²⁷. The fitting yielded values of $\alpha = 1.28$ and $l_\phi = 183\text{ nm}$, which agrees well with previous measurements for Bi_2Se_3 ^{39–41}.

To explore the differences between the superconducting bulk and non-superconducting thin-film samples, we performed atom-by-atom EDX mapping for both types of samples. Figure 3a and b present the EDX mappings for the superconducting $\text{Sr}_{0.05}\text{Bi}_2\text{Se}_3$ bulk (Sample A) and non-superconducting thin film $\text{Sr}_{0.13}\text{Bi}_2\text{Se}_3$ (Sample B), respectively. No clear differences were observed. Bi(Sr) substitutional and interstitial doping were detected inside the quintuple layers in both types of samples. The slight difference is that Sr dopant atoms intercalated in vdW gaps were frequently visible in the thin-film samples, whereas their presence in the bulk samples was relatively rare. This difference is mainly due to the technical difficulty in imaging the dopant atoms in vdW gaps. Because the dopant atoms are highly mobile in vdW gaps, the bulk samples with low Sr concentration ($\text{Sr}_{0.05}\text{Bi}_2\text{Se}_3$) can hardly generate signals in EDX mapping as strong as the thin-film samples with higher Sr concentration ($\text{Sr}_{0.13}\text{Bi}_2\text{Se}_3$) can.

Statistical method to determine the separations between adjacent Bi layers. To further explore the differences between the bulk and thin-film samples, we quantitatively evaluated the variation of the Bi_2Se_3 lattice structure along the c -axis. In addition to samples A and B, a pristine Bi_2Se_3 bulk sample (sample C) was prepared for comparison. We performed numerous measurements of the separation between two Bi layers inside the same quintuple layer (d1) and between the closest Bi layers in two neighbouring quintuple layers (d2) for these samples. To reduce any systematic errors, all the high-resolution HAADF-STEM images were obtained under the same experimental settings. The original images were fast Fourier filtered to reduce the noise, which also enhanced the image contrast. Because Bi atoms are much heavier than Se atoms, their intensity was higher. Thus, by setting an appropriate image intensity threshold, all the Bi atoms could be identified along with their atomic locations. The actual position of each individual atom was determined from the two-dimensional Gaussian peak fitting of the image intensity. Using the method described above, the separation between adjacent Bi atoms was

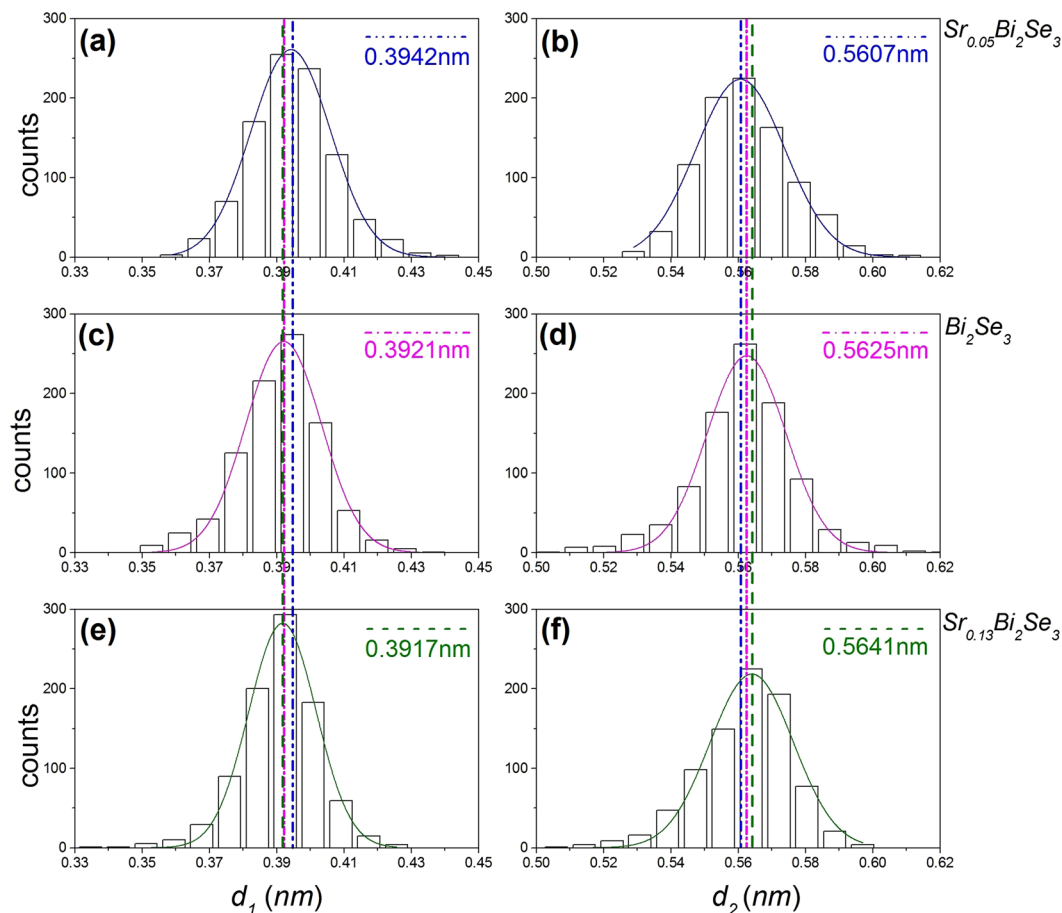


Figure 4. Statistics of the separation between Bi layers in the same quintuple layer (d_1) and between the closest Bi layers in two neighbouring quintuple layers (d_2). (a,b) $\text{Sr}_{0.05}\text{Bi}_2\text{Se}_3$ bulk sample; (c,d) pristine Bi_2Se_3 bulk sample; and (e,f) $\text{Sr}_{0.13}\text{Bi}_2\text{Se}_3$ thin-film sample. d_2 of the $\text{Sr}_{0.13}\text{Bi}_2\text{Se}_3$ thin-film sample was clearly expanded by 3.4 pm compared with that of the $\text{Sr}_{0.05}\text{Bi}_2\text{Se}_3$ bulk sample, whereas d_1 was compressed by 2.5 pm.

measured with picometre accuracy. Figure 4 presents a histogram of the separations d_1 and d_2 for samples A, B, and C. Using pristine Bi_2Se_3 as a reference, the Gaussian fitting of the histograms indicated that d_1 in $\text{Sr}_{0.05}\text{Bi}_2\text{Se}_3$ bulk was expanded by 2.1 pm, whereas d_2 was compressed by 1.8 pm; in contrast, in the thin-film sample, d_1 was compressed by 0.4 pm and d_2 was expanded by 1.6 pm. Therefore, the structural changes in the bulk and thin-film Sr-doped Bi_2Se_3 samples showed opposite trends of compression/expansion, as illustrated in Fig. 5.

Discussion

Why superconductivity is absent in doped TIs thin films has been elusive for a long time. The answer to this question is not only necessary to understand the origin of the superconductivity in doped TIs, but will also contribute to the successful growth of superconducting doped TI thin films, which are important for the study of exotic Majorana quasiparticles and the related quantum transport phenomena.

Initially, it was thought that dopants such as Cu atoms intercalated into vdW gaps acted as electron donors and that the superconductivity was generated merely through electron doping. Later experiments performed by Shirasawa *et al.*, however, did not support this speculation²³. Although Cu intercalation was confirmed in their thin Bi_2Se_3 film grown by MBE, the expected superconductivity did not appear. The authors concluded that the electron doping itself could not guarantee the emergence of superconductivity and that other effects such as inhomogeneity may also be vital for superconductivity. There were some suspicions, for example in Cu doped Bi_2Se_3 , that copper atoms might leak out to the surface, especially in thin-film and nano-flake samples, and the leakage of copper atoms would destroy the superconductivity. For example, Ribak *et al.* occasionally observed an extremely large band gap in Cu-doped Bi_2Se_3 superconducting bulk samples using angle-resolved photoemission spectroscopy⁴². They found through calculations that the application of a uniaxial internal stress along the c -axis could explain the increase of the band gap. They thought that the release of the stress in the layers close to the surface might explain why it was rare to observe such a large band gap in previous ARPES measurements. They claimed that the absence of superconductivity in exfoliated Bi_2Se_3 was also related with the release of the internal stress⁴².

In our experiments, we found that Sr doped Bi_2Se_3 thin-film samples resembled their bulk counterparts in many aspects. TEM inspection revealed good crystallinity of the thin-film samples, and magneto-resistance measurements confirmed the existence of a topological surface state. In addition, the carrier densities of the

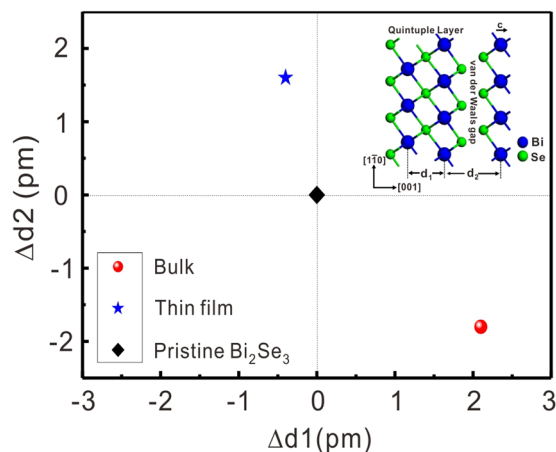


Figure 5. Lattice deformation deduced from STEM measurements. Variations of d_1 and d_2 in bulk and thin-film samples, with pristine Bi_2Se_3 used as a reference. d_1 is the spacing between two Bi layers in the same quintuple layer, and d_2 is the spacing between the closest Bi layers in two neighbouring quintuple layers. Inset: Schematic illustration of d_1 and d_2 in Bi_2Se_3 lattice.

thin-film samples were similar to those of the bulk Sr-doped Bi_2Se_3 samples. Even the EDX mappings did not reveal any clear differences in the Sr doping structures between the bulk and thin-film samples. Since our films are quite thick, it is unlikely that the absence of superconductivity is due to the direct tunnelling between the top and bottom surfaces^{43,44}. Because the superconducting properties of doped Bi_2Se_3 should be mainly affected by its doping structure, the emergence of superconductivity must be highly correlated with the subtle variations of Bi_2Se_3 lattice structure (One can also argue that the superconductivity is caused by an unknown impurity. But to date, no such impurity has been identified yet).

As the technique used in the growth of thin-film and bulk samples is very different, and the actual Sr concentration depends on many experimental details such as the choice of substrate, the environmental temperature during sample growth and the nominal Sr doping level, it will be very hard to get identical actual Sr concentration in thin-film and bulk samples to make a more robust comparison. We think that the best strategy is to turn a non-superconducting film into a superconducting one, then one can make a comparison of lattice constants between a superconducting film and a non-superconducting one grown under similar conditions. We noticed a recent work from Mlack *et al.* who used voltage pulse/thermal annealing to treat Bi_2Se_3 nano-flakes (approximately 100-nm-thick) capped with Pd electrodes^{45,46}. Although the superconducting behavior observed in the annealed flake was not very clean, this work shows promise that superconducting doped Bi_2Se_3 thin film is possible to get.

In summary, the emergence of superconductivity in doped Bi_2Se_3 should be highly correlated with the doping structure. Because no qualitative distinction between superconducting bulk and non-superconducting thin-film samples has been found, one should turn to quantitative structural analysis to understand the emergence of superconductivity in doped Bi_2Se_3 . Future work with better design of experiments is needed to reveal the relation between superconductivity and doping induced lattice structure changes.

Methods

Material Synthesis. $\text{Sr}_{0.05}\text{Bi}_2\text{Se}_3$ superconducting bulk materials were synthesised by melting a mixture of high-purity Bi, Se, and Sr with a nominal atomic ratio of 2:3:0.05. The mixture was prepared in a nitrogen glove box and then sealed in a quartz ampoule. The ampoule was heated at 850 °C for 24 h and then cooled to 620 °C at a rate of 3 °C/h. The samples were then quenched in ice water. The Sr-doped Bi_2Se_3 thin-film samples were grown by MBE on insulating $\text{SrTiO}_3(111)$ substrates. The substrates were heated at approximately 240 °C during film growth. Bi and Se were co-deposited onto the substrate with a flux ratio of ~20:1.

Sample Characterisation. The electrical measurements were performed in a helium-4 cryostat and in a dilution fridge using DC and the lock-in technique.

HRTEM Examination. Cross-sectional samples were prepared for HRTEM examination using a dual-beam microscope (FIB, Quanta 3D, FEG, FEI) with Ga ion milling and a precision ion-polishing system (Gatan 691) with Ar ion milling. The structural defects of the samples were examined with an FEI TITAN Cs-corrected ChemiSTEM operated at an acceleration voltage of 200 kV to avoid knock-on damage. HAADF-STEM analysis was performed using a spherical aberration probe-corrector to achieve a spatial resolution of up to 0.08 nm. The ChemiSTEM EDX provides outstanding sensitivity for determining elements at atomic resolution. To minimize the uncertainty of our measurements, sample drafting was well controlled in the experiments. Any data with an average drafting large than 0.1 pm/unit cell was excluded. To minimize the artificiality caused by different experimental conditions, the three samples reported in the text were measured successively in short delay and under nearly the same conditions, including the way of sample preparation, thickness of sample, magnification, camera length, pixel size, probe size, and so on.

References

- Castelvecchi, D. The shape of things to come. *Nature* **547**, 272–274 (2017).
- Qi, X.-L. & Zhang, S.-C. Topological insulators and superconductors. *Rev. Mod. Phys.* **83**, 1057–1110 (2011).
- Ando, Y. & Fu, L. Topological Crystalline Insulators and Topological Superconductors: From Concepts to Materials. *Annu. Rev. Condens. Matter Phys.* **6**, 361–381 (2015).
- Alicea, J. *et al.* Non-Abelian statistics and topological quantum information processing in 1D wire networks. *Nat. Phys.* **7**, 412–417 (2011).
- Wilczek, F. Majorana returns. *Nat. Phys.* **5**, 614–618 (2009).
- Beenakker, C. W. J. Search for Majorana Fermions in Superconductors. *Annu. Rev. Condens. Matter Phys.* **4**, 113–136 (2013).
- Hor, Y. S. *et al.* Superconductivity in $\text{Cu}_x\text{Bi}_2\text{Se}_3$ and its implications for pairing in the undoped topological insulator. *Phys. Rev. Lett.* **104**, 057001 (2010).
- Liu, Z. *et al.* Superconductivity with Topological Surface State in $\text{Sr}_x\text{Bi}_2\text{Se}_3$. *J. Am. Chem. Soc.* **137**, 10512 (2015).
- Qiu, Y. *et al.* Time reversal symmetry breaking superconductivity in topological materials. *arXiv* **1512**, 03519 (2015).
- Sasaki, S. *et al.* Topological Superconductivity in $\text{Cu}_x\text{Bi}_2\text{Se}_3$. *Phys. Rev. Lett.* **107**, 217001 (2011).
- Matano, K. *et al.* Spin-rotation symmetry breaking in the superconducting state of $\text{Cu}_x\text{Bi}_2\text{Se}_3$. *Nat. Phys.* **12**, 852–854 (2016).
- Yonezawa, S. *et al.* Thermodynamic evidence for nematic superconductivity in $\text{Cu}_x\text{Bi}_2\text{Se}_3$. *Nat. Phys.* **13**, 123–126 (2016).
- Levy, N. *et al.* Experimental evidence for s-wave pairing symmetry in superconducting $\text{Cu}_x\text{Bi}_2\text{Se}_3$ single crystals using a scanning tunneling microscope. *Phys. Rev. Lett.* **110**, 117001 (2013).
- Wray, L. A. *et al.* Observation of topological order in a superconducting doped topological insulator. *Nat. Phys.* **6**, 855–859 (2010).
- Kriener, M. *et al.* Bulk superconducting phase with a full energy gap in the doped topological insulator $\text{Cu}_x\text{Bi}_2\text{Se}_3$. *Phys. Rev. Lett.* **106**, 127004 (2011).
- Kriener, M. *et al.* Electrochemical synthesis and superconducting phase diagram of $\text{Cu}_x\text{Bi}_2\text{Se}_3$. *Phys. Rev. B* **84**, 054513 (2011).
- Wang, M. *et al.* A combined method for synthesis of superconducting Cu doped Bi_2Se_3 . *Sci. Rep.* **6**, 22713 (2016).
- Teo, J. C. & Kane, C. L. Majorana fermions and non-Abelian statistics in three dimensions. *Phys. Rev. Lett.* **104**, 046401 (2010).
- Parhizgar, F. & Black-Schaffer, A. M. Highly tunable time-reversal-invariant topological superconductivity in topological insulator thin films. *Sci. Rep.* **7**, 9817 (2017).
- Phong, V. T. *et al.* Majorana zero modes in a two-dimensional p-wave superconductor. *Phys. Rev. B* **96**, 060505 (2017).
- Sun, H.-H. & Jia, J.-F. Detection of Majorana zero mode in the vortex. *npj Quantum Materials* **2**, 34 (2017).
- Potter, A. C. & Fu, L. Anomalous supercurrent from Majorana states in topological insulator Josephson junctions. *Phys. Rev. B* **88**, 121109 (2013).
- Shirasawa, T. *et al.* Structure and transport properties of Cu-doped Bi_2Se_3 films. *Phys. Rev. B* **89**, 195311 (2014).
- Li, M. *et al.* Electron delocalization and relaxation behavior in Cu-doped Bi_2Se_3 films. *Phys. Rev. B* **96**, 075152 (2017).
- Takagaki, Y. *et al.* Weak antilocalization and electron-electron interaction effects in Cu-doped Bi_2Se_3 films. *Phys. Rev. B* **85**, 115314 (2012).
- Gao, B. F. *et al.* Gate-controlled linear magnetoresistance in thin Bi_2Se_3 sheets. *Appl. Phys. Lett.* **100**, 212402 (2012).
- Wang, Z. *et al.* Linear magnetoresistance versus weak antilocalization effects in Bi_2Te_3 . *Nano Research* **8**, 2963–2969 (2015).
- Veldhorst, M. *et al.* Magnetotransport and induced superconductivity in Bi based three-dimensional topological insulators. *Phys. Status Solidi RRL* **7**, 26–38 (2013).
- Bao, L. *et al.* Weak anti-localization and quantum oscillations of surface states in topological insulator $\text{Bi}_2\text{Se}_2\text{Te}$. *Sci. Rep.* **2**, 726 (2012).
- He, H. T. *et al.* Impurity effect on weak antilocalization in the topological insulator Bi_2Te_3 . *Phys. Rev. Lett.* **106**, 166805 (2011).
- Shruti *et al.* Superconductivity by Sr intercalation in the layered topological insulator Bi_2Se_3 . *Phys. Rev. B* **92**, 020506 (2015).
- Hikami, S. *et al.* Spin-Orbit Interaction and Magnetoresistance in the Two Dimensional Random System. *Prog. Theor. Phys.* **63**, 707 (1980).
- Adroguer, P. *et al.* Conductivity corrections for topological insulators with spin-orbit impurities: Hikami-Larkin-Nagaoka formula revisited. *Phys. Rev. B* **92**, 241402(R) (2015).
- Liu, W. E. *et al.* Weak Localization and Antilocalization in Topological Materials with Impurity Spin-Orbit Interactions. *Materials* **10**, 807 (2017).
- Han, C. Q. *et al.* Electronic structure of a superconducting topological insulator Sr-doped Bi_2Se_3 . *Appl. Phys. Lett.* **107**, 171602 (2015).
- Kim, D. *et al.* Coherent topological transport on the surface of Bi_2Se_3 . *Nat. Commun.* **4**, 2040 (2013).
- Singh, S. *et al.* Quantum and classical contributions to linear magnetoresistance in topological insulator thin films. *AIP Conf. Proc.* **1728**, 020557 (2016).
- Wang, X. *et al.* Room Temperature Giant and Linear Magnetoresistance in Topological Insulator Bi_2Te_3 Nanosheets. *Phys. Rev. Lett.* **108**, 266806 (2012).
- Matsuo, S. *et al.* Weak antilocalization and conductance fluctuation in a submicrometer-sized wire of epitaxial Bi_2Se_3 . *Phys. Rev. B* **85**, 075440 (2012).
- Pan, H. *et al.* Nontrivial surface state transport in Bi_2Se_3 topological insulator nanoribbons. *Appl. Phys. Lett.* **110**, 053108 (2017).
- Jing, Y. *et al.* Weak antilocalization and electron-electron interaction in coupled multiple-channel transport in a Bi_2Se_3 thin film. *Nanoscale* **8**, 1879–1885 (2016).
- Ribak, A. *et al.* Internal pressure in superconducting Cu-intercalated Bi_2Se_3 . *Phys. Rev. B* **93**, 064505 (2016).
- Liu, W. E. *et al.* Screening, Friedel oscillations, and low-temperature conductivity in topological insulator thin films. *Phys. Rev. B* **89**, 195417 (2014).
- Shan, W.-Y. *et al.* Effective continuous model for surface states and thin films of three-dimensional topological insulators. *New J. Phys.* **12**, 043048 (2010).
- Mlack, J. T. G. and Low Temperature Transport Measurements of Pure and Doped Bismuth Selenide. *PhD Dissertation* (2015).
- Mlack, J. T. *et al.* Patterning Superconductivity in a Topological Insulator. *ACS Nano* **11**, 5873–5878 (2017).

Acknowledgements

We thank W. Li and M.Y for helpful discussions. This work was supported by National Natural Science Foundation of China under Grant No. 11374321, No. 11474249, No. U1632272, No. U1632266, No. 11574201, No. 11521404 and No. 11227902; by Ministry of Science and Technology of China under Grant No. 2016YFA0301003; by the National 973 Program of China under Grant No. 2015CB654901, by The National Key Research and Development Program of China under Grant 2017YFB0703100. H.T. acknowledges support from Young 1000 Talents Program of China. D.Q. acknowledges support from the Changjiang Scholars Program.

Author Contributions

C. Han and W. Jiang grew the thin-film samples, M. Wang and Z. Li performed structural and electrical measurements, D. Zhang performed the TEM inspections and data analysis. M. Wang, C. Han and D. Zhang contributed equally to this work. J. Jia, J. Li and S. Qiao contributed to the discussions. D. qian, H. Tian and B. Gao designed the experiment and wrote the manuscript.

Additional Information

Competing Interests: The authors declare that they have no competing interests.

Publisher's note: Springer Nature remains neutral with regard to jurisdictional claims in published maps and institutional affiliations.



Open Access This article is licensed under a Creative Commons Attribution 4.0 International License, which permits use, sharing, adaptation, distribution and reproduction in any medium or format, as long as you give appropriate credit to the original author(s) and the source, provide a link to the Creative Commons license, and indicate if changes were made. The images or other third party material in this article are included in the article's Creative Commons license, unless indicated otherwise in a credit line to the material. If material is not included in the article's Creative Commons license and your intended use is not permitted by statutory regulation or exceeds the permitted use, you will need to obtain permission directly from the copyright holder. To view a copy of this license, visit <http://creativecommons.org/licenses/by/4.0/>.

© The Author(s) 2018